Indonesian Physical Review
Volume 09 Issue 01, January 2026
P-ISSN: 2615-1278, E-ISSN: 2614-7904

First Principles Study on Electronic and Optical Properties of CoX (X=Cr, Mn, Ti, V) co-doped ZnO Semiconductor

Harry Prayoga[1], Abdul Rajak[1], Agustina Widiyani[1], Priyan Prayogo[1], Fatimatul Musfiroh[2], Indra Pardede[1*]

[1]*Master Physics Department, Faculty of Science, Sumatera Institute of Technology, Lampung Selatan, Lampung, Indonesia*

[2]*Physics Department, Faculty of Science, Sumatera Institute of Technology, Lampung Selatan, Lampung, Indonesia*

Corresponding Author's E-mail: indra.pardede@fi.itera.ac.id

Article Info

Article info:
Received: 16-07-2025
Revised: 17-11-2025
Accepted: 24-11-2025

Keywords:
absorbance; bandgap; d-orbital; DFT; DFT+U

How To Cite:
H. Prayoga, A. Rajak, A. Widiyanti, P. Prayogo, F. Musfiroh, and I. Pardede. "First-Principles Study on Electronic and Optical Properties of CoX (X = Cr, Mn, Ti, V) co-doped ZnO Semiconductor", Indonesian Physical Review, vol. 9, no. 1, pp. 58–78, 2026.

DOI:
https://doi.org/10.29303/ipr.v9i1.530

Abstract

The development of solar energy materials is essential for achieving the Sustainable Development Goals (SDGs). However, their performance is often limited by the electronic and optical properties of commonly used semiconductors. Unlike previous DFT studies mostly focused on non–transition metal dopants (e.g., Al, Ga), this work explores pristine ZnO, single cobalt (Co) doping, and CoX (X = chromium (Cr), manganese (Mn), titanium (Ti), and vanadium (V)) codoping to reveal how single and dual 3d-orbital interactions modify its electronic and optical behavior. This study investigates the effects of transition metal codoping CoX (X = Cr, Mn, Ti, V) on ZnO using Density Functional Theory (DFT) and DFT with Hubbard U correction (DFT+U) within the Generalized Gradient Approximation (GGA) to evaluate opto-electronic properties. The bandgap of pristine ZnO was calculated as ~0.80 eV with standard DFT, while ZnO-Co and ZnO-CoX exhibited zero bandgap with a flatband due to conduction band overlap with the Fermi level, indicating metallic behavior resulting from d-orbital contributions. DFT+U improved the pristine ZnO bandgap to ~1.08 eV, although Co-doped and CoX co-doped remained metallic. Orbital resolved analysis shows that Ti and V introduce states near the valence band, while Cr and Mn shift states deeper below the Fermi level, reflecting distinct d-orbital interactions. The theoretical band gaps underestimated experimental values due to strong electron correlation in ZnO. Optical analysis revealed that Co and CoX codoping shifts the absorption edge into the visible range and enhances the absorption intensity. The presence of dopants alters the electronic band structure and enhances optical absorption in the visible range, underscoring their effectiveness in engineering ZnO-based semiconductors for optimized optoelectronic responses.

Introduction

Clean energy development relies heavily on the discovery of semiconducting materials that can efficiently convert solar radiation into electricity. Fossil fuels remain the dominant source of global energy, prompting efforts to shift toward sustainable alternatives [1]. Solar energy provides a carbon-neutral and abundant power source, with high availability in tropical regions like Indonesia. [2]. It also plays a key role in driving secondary renewables such as wind and hydro energy [3–4].

Among the various photovoltaic technologies, solar cells based on silicon, dye-sensitized, and perovskite materials have attracted attention, with perovskites offering high conversion efficiency despite their instability issues [5-8]. Zinc Oxide (ZnO) is a promising candidate for next-generation photovoltaics due to its wide band gap, optical transparency, and low toxicity, which also enhance its electrical conductivity and light absorption capabilities [9–10]. ZnO's performance can be further enhanced through doping with transition metals, such as cobalt, to increase the free carrier density via shallow donor states and enable light absorption within the visible range (400–600 nm) [11–12]. However, the synergistic effects of codoping ZnO with combinations of transition metals, particularly involving Co and elements like Cr, Mn, Ti, and V, remain poorly understood and insufficiently studied. Cr, Mn, Ti, and V were chosen as codopants because their distinct 3*d* electronic configurations can introduce localized *d*-orbital states in ZnO's band structure. These dopants have different ionic radii and valence states, which affect defect formation energies, hybridization with ZnO states, and optical transitions. This makes them suitable for systematically investigating the effects of transition-metal codoping on the electronic and optical properties of ZnO.

However, most previous first-principles studies have been limited to single dopant systems or employed standard Density Functional Theory (DFT), often underestimating band gaps and optical transitions. Recent works using DFT+U or hybrid functionals have improved accuracy but remain focused on isolated dopants, leaving the synergistic effects of transition-metal codoping largely unexplored. Unlike previous studies that focused on specific codopant pairs, this work provides a comparative understanding of multiple transition-metal codoping combinations within a unified computational framework.

In this study, we systematically investigate the impact of codoping ZnO with cobalt and a secondary transition metal (Cr, Mn, Ti, V) on its electronic and optical properties using DFT and DFT+U calculations. Using first-principles DFT and DFT+U calculations, the band structure and absorption of ZnO codoped with CoX (X = Cr, Mn, Ti, V) are systematically evaluated. Unlike previous studies that focus on isolated dopants or a narrow set of codoping cases, this work compares multiple CoX configurations under consistent simulation parameters, allowing for a detailed analysis of *d*-orbital hybridization and band structure modulation. Codoping is expected to introduce localized electronic states that modify the conduction and valence band edges, potentially enhancing absorption in the visible light region [12]. These findings provide fundamental insights into codoping strategies for tailoring ZnO-based semiconductors and demonstrate their potential application in photovoltaic and optoelectronic devices.

Theoretical Background

ZnO has attracted considerable research interest due to its wide band gap and high electrical conductivity. Doping with transition metals such as Co, Cu, and Ni can alter their magnetic and optical properties by modifying the band structure and charge carrier distribution [13,14]. Since 2021, codoping strategies, where two or more dopants are introduced simultaneously, have emerged to further tailor the electronic and optical properties of ZnO. Codoping with elements like Al–F, Ga–F, or In–F has shown improved conductivity and reduced charge carrier relaxation time [15].

Computational approaches, particularly Density Functional Theory (DFT), have become crucial in predicting these effects prior to experimental synthesis, thereby saving both time and cost. For example, in 2023, ZnO co-doped with Co and Mn using the LDA+U method demonstrated enhanced magnetic properties [16], while DFT with the LDA-PBE functional revealed that Co doping introduces a magnetic moment of ~3.073 μB [17]. These characteristics are beneficial for spintronic applications where magnetic ordering and reduced band gap are desired [18-19]. Additionally, doping with rare-earth elements or codoping with Li–F and Co–Gd has shown potential for enhancing ZnO's properties in optoelectronic applications such as light-emitting diodes and photoactive materials [20–22]. Similar model studies on transition metals, particularly Ni, revealed that magnetic surface anisotropy strongly depends on the effective potential changes of the 3*d* orbitals [23].

We employed spin-polarized DFT+U calculations to account for the strong electron correlation in ZnO–transition metal systems. The Perdew–Burke–Ernzerhof (PBE) functional within the GGA framework was used, with Hubbard U corrections applied to the 3*d* orbitals of transition-metal dopants, as detailed in the methodology. In DFT, the total energy of an interacting many-electron system is a functional of the electron density $n(\boldsymbol{r})$. The Kohn–Sham equations are obtained by mapping this system onto non-interacting electrons in an effective potential, allowing the total energy to be written as:

$$E[n] = \sum_{\substack{i=1 \\ \varepsilon_i \le E_F}}^{N} \varepsilon_i - \int\int \frac{n(\boldsymbol{r})n(\boldsymbol{r}')}{|\boldsymbol{r}-\boldsymbol{r}'|} d\boldsymbol{r}\, d\boldsymbol{r}' - \int n(\boldsymbol{r})\, V_{xc}(\boldsymbol{r}) d\boldsymbol{r} + \tilde{\mathrm{E}}_{\mathrm{xc}}[n] \qquad (1)$$

where ε_i are the Kohn–Sham eigenvalues, E_F is the Fermi level, $n(\boldsymbol{r})$ is the electron density, and $\tilde{\mathrm{E}}_{xc}$ is the approximation exchange-correlation energy. While this formulation has proven effective for many systems [32], it typically underestimates the bandgap of semiconductors, especially transition metal oxides such as ZnO. To address this limitation, we apply the DFT+U method, which introduces a Hubbard-like on-site Coulomb interaction U to partially correct the self-interaction errors inherent in standard DFT functionals. The corrected energy functional is:

$$E_{\mathrm{DFT+U}} = E_{\mathrm{DFT}} + \frac{U_{eff}}{2} \sum_{i,\sigma} [n_{i,\sigma}(1 - n_{i,\sigma})] \qquad (2)$$

where $U_{eff} = U - J$ is the effective on-site Coulomb parameter, and $n_{i,\sigma}$ is the occupation number of the localized *d*-orbitals for atom i and spin σ. This correction enhances the

description of localized states and improves the estimation of the band structure and optical transitions in ZnO-based semiconductors.

One of the key outputs of DFT simulations is the electronic band structure, which enables the calculation of the band energy. The summation runs over all occupied bands and **k**-points in the Brillouin zone. From this, the band gap E_{gap} can be determined, which is defined as:

$$E_{\text{gap}} = E_{\text{CBM}} - E_{\text{VBM}} \tag{3}$$

where E_{CBM} and E_{VBM} represent the conduction band minimum and valence band maximum, respectively. The band gap plays a critical role in determining whether a material behaves as a metal, semiconductor, or insulator. Understanding the distribution of electronic states is crucial for describing how a material interacts with incident light, particularly through its dielectric response. The density of states (DOS) provides insight into both the electronic and optical properties of a material [24]. Optical absorption was calculated from the complex dielectric function, where the imaginary part accounts for interband transitions, and the real part was obtained via the Kramers–Kronig transformation. These allow identification of absorption onset and peak features in the visible spectrum [25]. The material's complex dielectric constant is defined as $\varepsilon = \varepsilon_r + \varepsilon_i$, with $\varepsilon_r = \boldsymbol{n}^2 - \boldsymbol{k}^2$ and $\varepsilon_i = 2\boldsymbol{nk}$. In optical properties, such as the absorption spectrum, are derived from the complex dielectric function using the following expression:

$$\alpha = \frac{2\omega}{c}\sqrt{\frac{\sqrt{(\varepsilon_r)^2 + (\varepsilon_i)^2} - \varepsilon_r}{2}} \tag{4}$$

where α is the absorption spectrum, ε_r and ε_i are the real and imaginary parts of the dielectric constant, respectively, ω is the angular frequency, and c is the speed of light. These theoretical considerations support our interpretation of how codoping strategies modify ZnO's optical and electronic characteristics.

Computational Method

Density Functional Theory (DFT) is widely employed to predict the electronic and optical properties of semiconductors and transition metal oxides, including ZnO [26–28]. While other computational methods, such as Molecular Dynamics (MD) [29], support broader materials modeling, this study specifically focuses on pristine ZnO, Co-doped ZnO, and CoX-codoped ZnO (X = Cr, Mn, Ti, V). These configurations were selected due to their potential to modulate the band structure and enhance optical absorption, with a critical research gap regarding the lack of systematic studies on codoping strategies [30]. To address the bandgap underestimation inherent in standard DFT, particularly for systems involving strongly correlated *d*-electrons, we employed the DFT+U approach. A Hubbard U value of 3.3 eV was applied to the Co 3*d* orbitals, while a value of 4.0 eV was assigned to Cr, Mn, Ti, and V, following previous theoretical studies. The U correction was applied exclusively to the 3*d* orbitals of the transition metals [34]. Hybrid functionals such as HSE06 were not employed due to their high computational cost. The DFT+U method was deemed sufficient to capture the relative trends in band structure and optical responses across the doped ZnO systems.

This research focused on pristine ZnO, ZnO doped with Co, and ZnO co-doped with transition metals CoX. All calculations were performed using the Quantum Espresso (QE) [31], employing the Perdew–Burke–Ernzerhof (PBE) exchange-correlation functional [32]. A 2×2×2 wurtzite ZnO supercell containing 16 Zn and 16 O atoms was constructed using VESTA. All atomic positions and lattice parameters were fully relaxed until the forces converged, as shown in Figure 1.

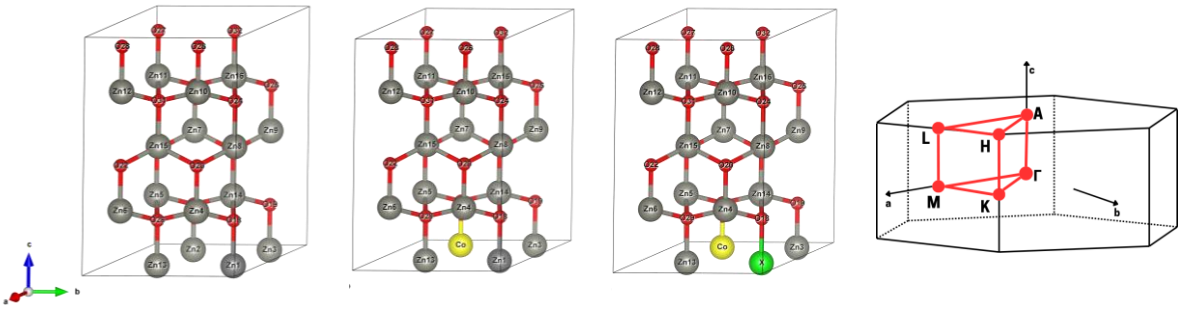

Figure 1. Structures of (a) pristine ZnO, (b) ZnO-Co, (c) ZnO-CoX, and (d) Brillouin zone showing the high-symmetry path Γ–M–K–Γ–A–L–H–A

Codoping was modeled by substituting one Zn atom with Co and another with X (X = Cr, Mn, Ti, or V), corresponding to a dopant concentration of 3.125% for each element. A 2×2×2 ZnO supercell, containing 32 atoms, was employed as a balanced model that accurately captures local structural distortion and dopant-induced electronic interactions while keeping computational costs reasonable. This configuration is widely used in first-principles studies of doped ZnO, as it sufficiently represents the dilute doping limit. The average dopant–dopant separation of ~9 Å effectively minimizes artificial periodic interactions among dopant images within the simulation cell. Although larger supercells could further reduce these effects, test calculations on total energy and density of states within the 2×2×2 model exhibited stable trends, indicating adequate convergence for this study. Therefore, this supercell model was deemed suitable for investigating the effects of single and codoping on the electronic and optical properties of ZnO. The optimized structural parameters and Brillouin Zone settings used for these calculations are described as follows.

The lattice parameters were set to $a = b = 6.44$ Å, $c = 10.4$ Å, with angles $\alpha = \beta = 90°$ and $\gamma = 120°$, consistent with the hexagonal symmetry [33]. The Brillouin Zone (BZ) of hexagonal ZnO, defined by its reciprocal lattice symmetry, begins and ends at the Γ point. In Figure 1(d), the lines in the diagram represent the k-point sampling, while the red paths highlight high-symmetry directions within the irreducible first BZ, describing the relationship between energy and electron momentum used in band structure calculations. The high-symmetry path Γ–M–K–Γ–A–L–H–A was selected because it represents the full symmetry of the wurtzite-type hexagonal structure, allowing comprehensive mapping of the electronic band dispersion. This path also follows the convention recommended by SeeK-path. Norm-conserving pseudopotentials from the *PseudoDojo library* (version 0.5.1) were used, with semicore states included for transition metal dopants. Optical properties were derived from the imaginary part of the dielectric function. The imaginary part was calculated using the independent particle approximation, which is suitable for describing interband transitions within DFT-level simulations. Energy convergence tests were conducted for the

cutoff energy and k-point density. An energy cut-off of 60 eV and a 7×7×5 k-point mesh was selected, where total energy differences had plateaued. Additional tests confirmed a stable dielectric response beyond this threshold.

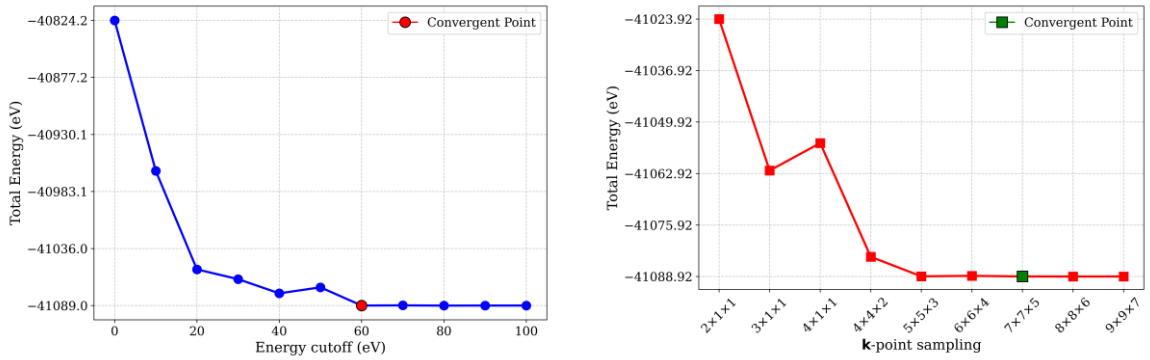

(a) **(b)**

Figure 2. Convergence tests: (a) total energy (eV) vs. cutoff energy (eV); (b) total energy (eV) vs. k-point mesh. Each system contains 32 atoms

Result and Discussion

This study aims to investigate the electronic and optical properties of the material using first-principles calculations. At the atomic scale, the complex many-body interactions among electrons and nuclei make solving the Schrödinger equation directly impractical. The Kohn-Sham formulation of DFT, as presented in Equation 1, addresses this by modeling the interacting electron system as non-interacting particles moving in an effective potential, which leads to the formation of electronic energy bands, including the valence band maximum and the conduction band minimum. These bands govern the material's electronic behavior, where the band gap, defined by the energy difference between the conduction band minimum and the valence band maximum, determines its conductivity. The density of states provides insight into the distribution of available electronic states and their role in charge transport. Optical properties, linked to electronic transitions between these bands, can be analyzed through the material's dielectric response and the resulting absorption coefficient presented in Equation 4.

Electronic Properties

The optimization of energy cutoff and **k**-point parameters was conducted to ensure convergence and accuracy in Density Functional Theory (DFT) calculations, using wurtzite ZnO as a reference prior to Co and transition metal doping, such as Cr, Mn, Ti, and V. After optimizing the energy cutoff and **k**-point parameters, DFT calculations were employed to investigate the electronic properties of ZnO.

As depicted in Figure 3(a), the calculated band structure reveals a band gap of ~0.80 eV, significantly lower than the experimental value of 3.23 eV [35]. This underestimation arises from the standard DFT's inability to properly describe systems with strongly correlated electron interactions. The DFT+U method introduces an on-site Coulomb correction to account for these interactions, leading to more accurate electronic structure predictions [34]. To address this, the DFT+U method was applied, exhibiting an increased band gap of ~1.08 eV, as shown in Figure 3(b). This method incorporates on-site Coulomb interactions with exchange-

correlation to better capture electron correlation effects. The DOS analysis further supports this result, with the DFT+U method yielding a smoother distribution near the Fermi level compared to the sharp peak observed in standard DFT. Figures 3(c) and 3(d) illustrate the electronic structure of Co-doped ZnO obtained using both DFT and DFT+U approaches. Co-doping introduces impurity states near the Fermi level, resulting in a reduced band gap. In some configurations, the band edges shift below the Fermi level, indicating a transition toward metallic behavior.

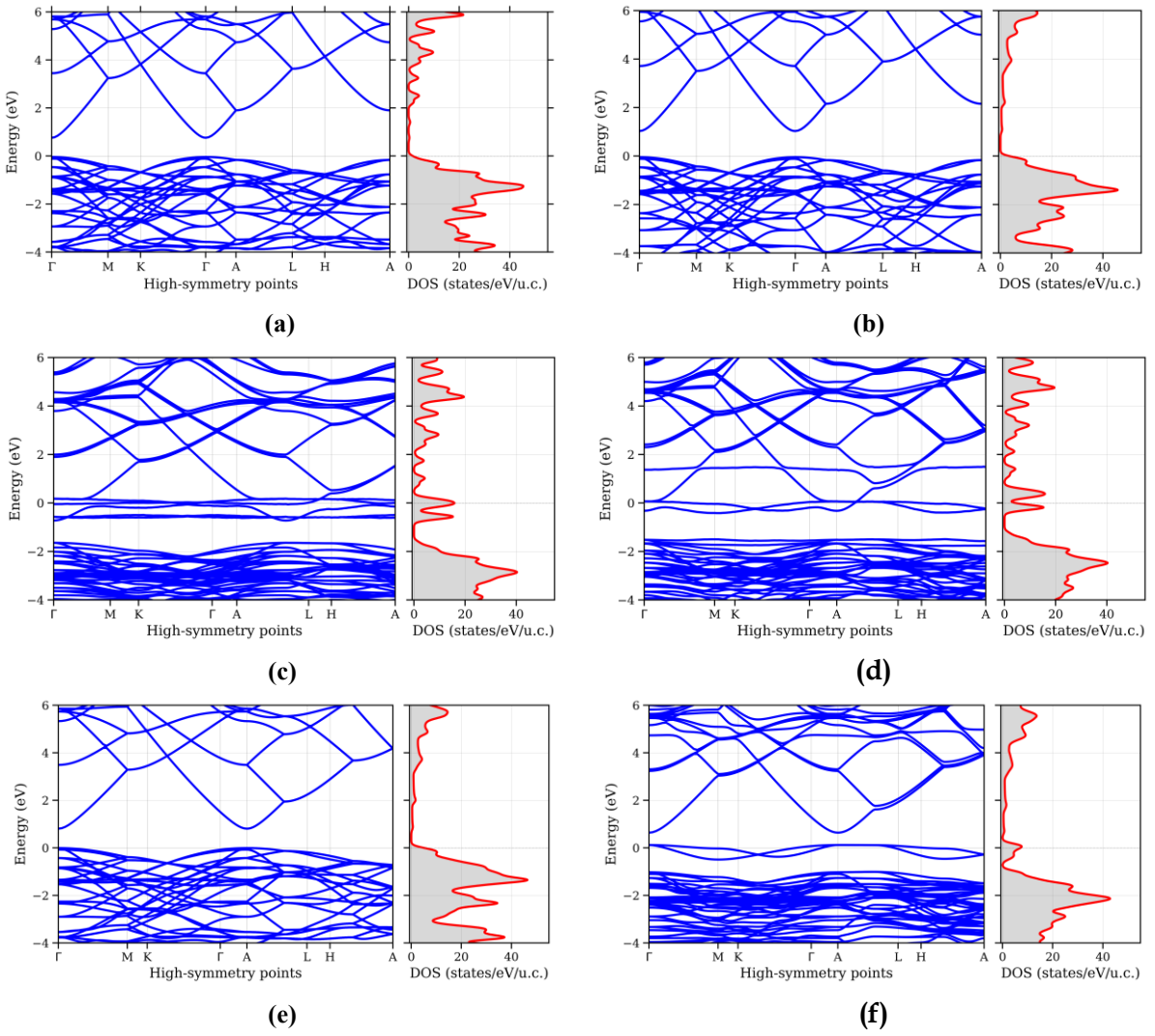

Figure 3. Electronic band structures of pristine and Co-doped ZnO calculated using DFT and DFT+U methods. (a) Pristine ZnO obtained from DFT, showing a band gap of ~0.8 eV; (b) Pristine ZnO with DFT+U, exhibiting an increased gap of ~1.08 eV; (c) Co-doped ZnO calculated using DFT, indicating metallic behavior due to band overlap at the Fermi level; (d) Co-doped ZnO with DFT+U, retaining metallic features; (e) Orbital-specific DFT+U result for pristine ZnO with U = 10 eV (Zn 3*d*) and 7 eV (Co 3*d*), showing a band gap of ~0.82 eV; and (f) Corresponding Co-doped ZnO structure, displaying flattened bands and metallic characteristics.

Standard DFT and DFT+U methods tend to underestimate the band gap and electronic structure, as they apply the Hubbard U correction at the atomic level. To improve accuracy,

this study employs an orbital-specific DFT+U approach, utilizing U values of 10 eV for the 3d Zn orbitals and 7 eV for the 3d Co orbitals, respectively. As illustrated in Figure 3 (e–f), the orbital-specific DFT+U results show more pronounced band dispersion for both pristine and Co-doped ZnO, indicating improved treatment of localized *d*-electrons. This approach yields a band gap of approximately 0.82 eV for pristine ZnO, which is higher than those obtained using standard DFT and atom-centered corrections. In contrast, the Co-doped system retains a zero-band gap with flattened bands, consistent with its metallic nature. Although orbital-specific corrections enhance the electronic description, the predicted values remain underestimated relative to experiment.

The electronic band structures of ZnO doped CoX (X = Cr, Mn, Ti, V), calculated using standard DFT, are presented in Figure 5. In all configurations, the Fermi level intersects the conduction band, indicating a collapse of the band gap and the emergence of metallic behavior. CoX codoping introduces additional electronic states near the Fermi level, significantly altering the band edge positions and effectively filling the band gap, thereby inducing metallic behavior.

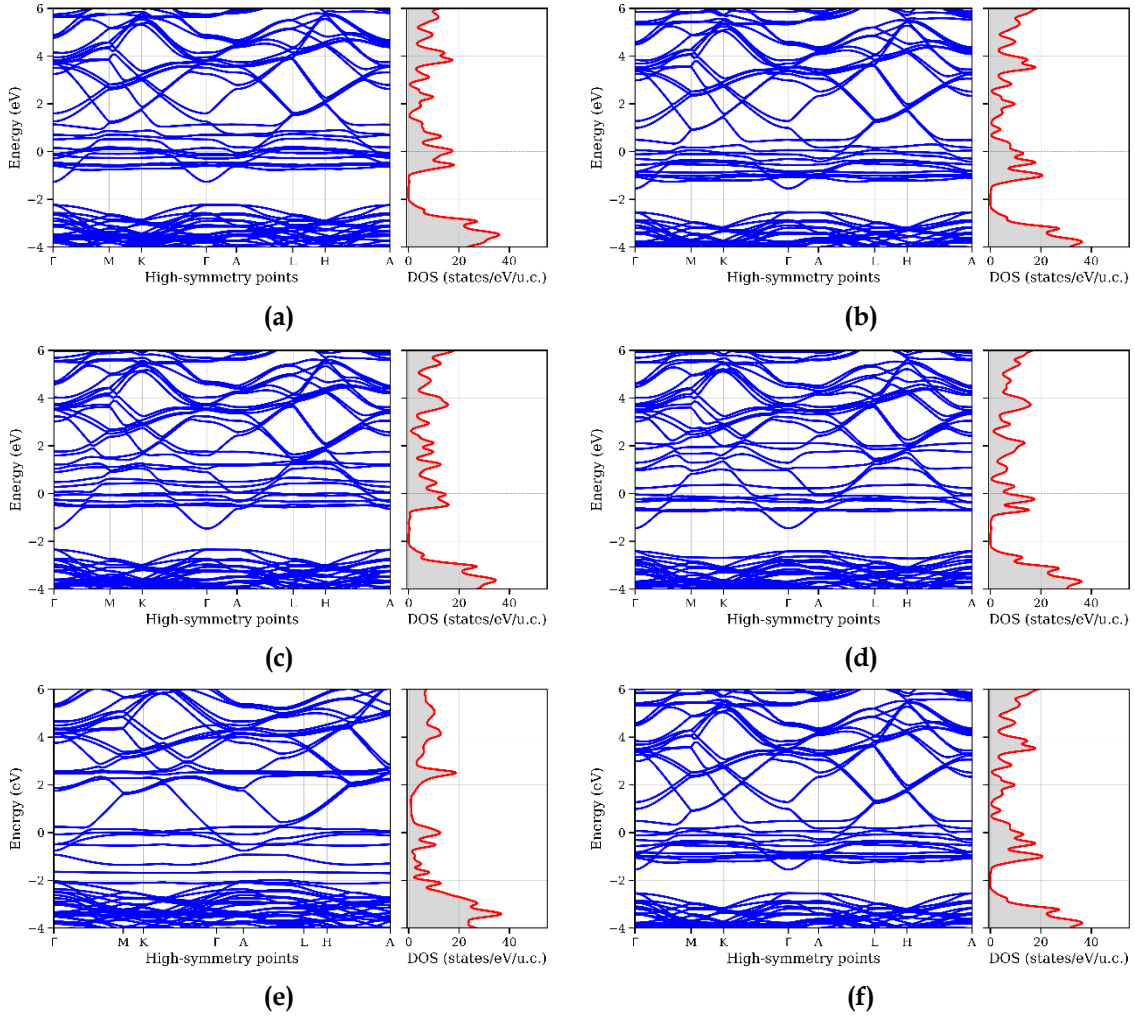

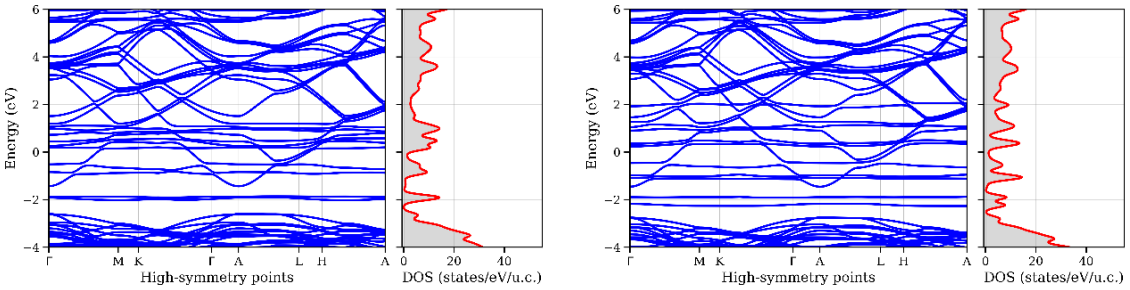

Figure 4. Band structures of CoX-doped ZnO (X = Cr, Mn, Ti, V) calculated using (a–d) standard DFT and (e–h) DFT+U with a U value of 4 eV applied to Zn and Co. Codoping modifies the electronic states near the Fermi level, showing band gap narrowing and increased DOS intensity, consistent with metallic behavior.

As shown in Figure 4, the band structures of CoX-codoped ZnO (X = Cr, Mn, Ti, V) obtained using the DFT+U method reveal that the Fermi level remains pinned within the conduction band, confirming the persistence of metallic behavior in all configurations. The inclusion of the on-site Hubbard U correction slightly reduces the density of states near the Fermi level, yet the band gap remains closed due to the strong hybridization between Co–X 3*d* and O 2*p* orbitals. This hybridization produces delocalized electronic states that bridge the valence and conduction bands, preventing the reopening of the gap even after partial electron localization is restored by the U correction. The metallic features observed in Co–Cr and Co–Mn systems are mainly associated with occupied t_{2g} states overlapping the Fermi level, whereas Co–Ti and Co–V introduce unoccupied 3*d* states just above it. These orbital interactions account for the observed narrowing of the band gap and the enhanced conductivity. Although the DFT+U correction mitigates self-interaction errors and improves the overall electronic description, both GGA and GGA+U approaches still underestimate the experimental band gap values, as summarized in Table 1, which compares the calculated electronic band gaps of ZnO CoX (X = Cr, Mn, Ti, V) using DFT and DFT+U.

Table 1 presents a comparison of the electronic band gap values of ZnO CoX materials, calculated using standard DFT, DFT+U, and experimental methods. The DFT+U method enhances band gap predictions by incorporating on-site Coulomb corrections with exchange-correlation to more accurately account for localized *d*-electron interactions; however, both methods still tend to underestimate the band gap compared to experimental values. Standard DFT often predicts metallic behavior in ZnO-Co and ZnO-Co X (X = Cr, Mn, Ti, V) due to its inability to fully capture electron correlation effects in these transition metal-doped systems [36]. Although DFT+U reduces these inaccuracies and provides a more reliable description of the electronic structure, band structure diagrams of ZnO with single Co doping and CoX codoping show that both DFT and DFT+U calculations reveal a persistent presence of energy states at the Fermi level. This results in the conduction band intersecting the Fermi level, which confirms the metallic nature of the doped ZnO systems. To further understand the origin of these electronic states, an orbital-resolved analysis was conducted on atoms located near the doping sites. In the ZnO–Co configuration, the Co atom was substituted at the Zn1 site.

Table 1. Comparison of electronic band gaps of ZnO, ZnO-Co, and ZnO-CoX.

Material	Method	Hubbard						Eg (eV)	Software	References
		Atom				Orbital				
		Zn	O	Co	X	Zn_d	O_p			
ZnO	GGA	-	-	-	-	-	-	0.74	CASTEP	[34]
ZnO	GGA+U	-	-	-	-	15	6	1.25	CASTEP	[34]
ZnO	Experiment	-	-	-	-	-	-	3.23	-	[35]
ZnO	GGA	-	-	-	-	-	-	0.80	QE	This Research
ZnO	GGA+U	4	0	4	4	-	-	1.08	QE	This Research
ZnO	GGA+U	-	-	-	-	10	7	0.82	QE	This Research
ZnO-Co	GGA	-	-	-	-	-	-	0	WIEN2k	[36]
ZnO-Co	Experiment	-	-	-	-	-	-	3.05	-	[37]
ZnO-Co	GGA	-	-	-	-	-	-	0	QE	This Research
ZnO-Co	GGA+U	4	0	4	4	-	-	0	QE	This Research
ZnO-Co	GGA+U	-	-	-	-	10	7	0	QE	This Research
ZnO-CoCr	GGA	-	-	-	-	-	-	0	QE	This Research
ZnO-CoCr	GGA+U	4	0	4	4	-	-	0	QE	This Research
ZnO-CoMn	GGA	-	-	-	-	-	-	0	QE	This Research
ZnO-CoMn	GGA+U	4	0	4	4	-	-	0	QE	This Research
ZnO-CoTi	GGA	-	-	-	-	-	-	0	QE	This Research
ZnO-CoTi	GGA+U	4	0	4	4	-	-	0	QE	This Research
ZnO-CoV	GGA	-	-	-	-	-	-	0	QE	This Research
ZnO-CoV	GGA+U	4	0	4	4	-	-	0	QE	This Research

The projected orbital contributions were analyzed for neighboring atoms, including O17, which is directly bonded to Co, and Zn13, which is located near the Co dopant but does not form a direct bond. For the CoX co-doped systems, Co and the secondary dopant X, where X represents a transition metal (Cr, Mn, Ti, or V), replaced the Zn1 and Zn2 sites, respectively. Orbital-resolved analysis was then conducted on atoms adjacent to the dopants, specifically O18, which is directly bonded to the X dopant, and Zn3, which is in the vicinity of X but not directly bonded. Despite applying DFT+U to correct band gap underestimation in transition metal-doped ZnO, band structures still show states overlapping the Fermi level. This indicates the introduction of electronic states that may close the gap and affect ZnO's semiconducting behavior.

Their persistence after the on-site Coulomb correction suggests the need for a more localized electronic analysis to identify the orbitals responsible for these states. The projected density of states (PDOS) provides a detailed description of how individual atomic orbitals contribute to the total electronic structure, particularly near the Fermi level. This method enables the identification of the specific dopant or host atoms responsible for states affecting conductivity and band gap behavior. By examining the PDOS for both single Co doping and CoX (X = Cr, Mn, Ti, V) codoping configurations, the role of each transition-metal dopant in modifying ZnO's electronic structure can be systematically clarified.

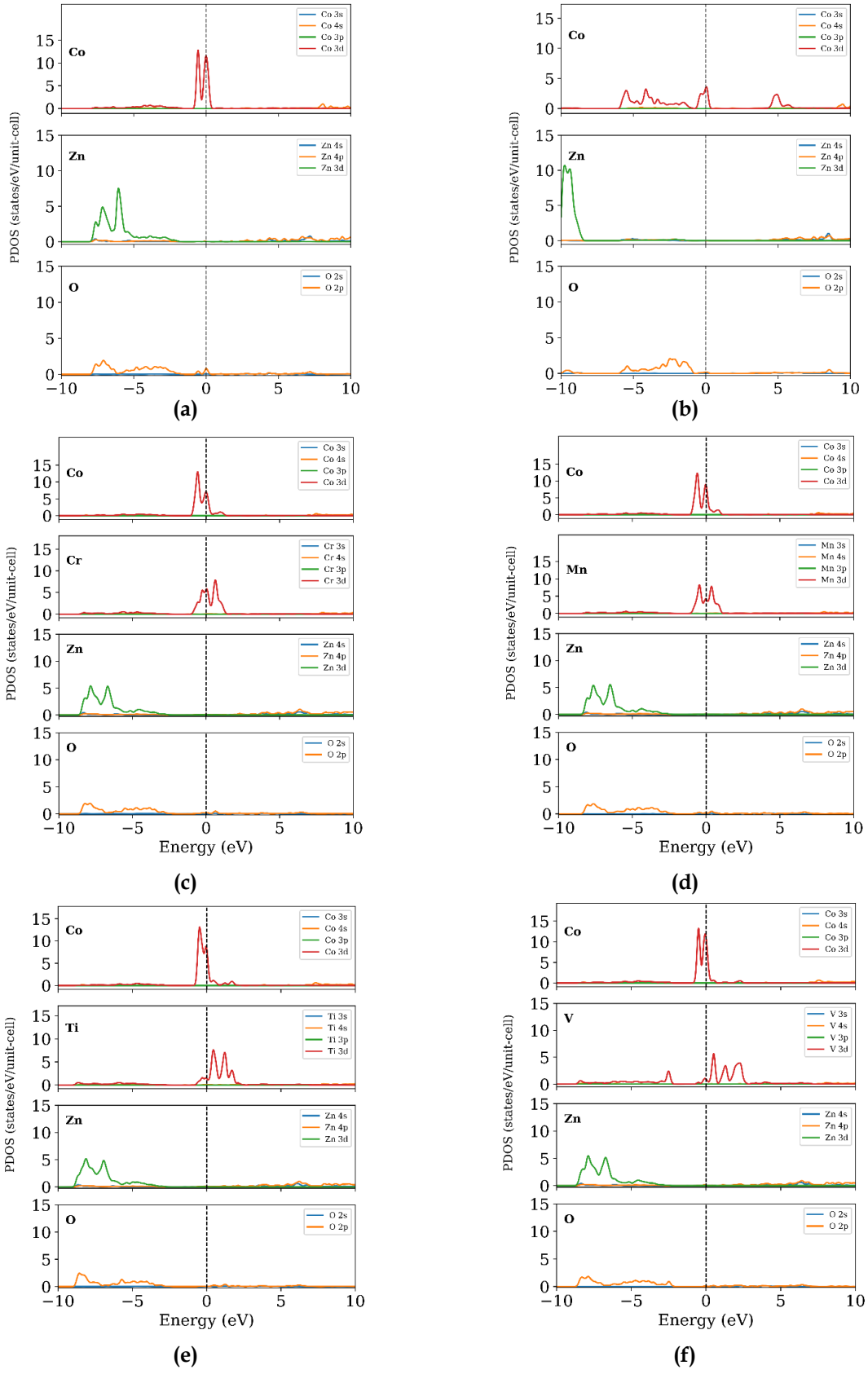
Co
Zn
O
Co 3s
Co 4s
Co 3p
Co 3d
Zn 4s
Zn 4p
Zn 3d
O 2s
O 2p
PDOS (states/eV/unit-cell)
(a)
(b)
Cr
Cr 3s
Cr 4s
Cr 3p
Cr 3d
Mn
Mn 3s
Mn 4s
Mn 3p
Mn 3d
Energy (eV)
(c)
(d)
Ti
Ti 3s
Ti 4s
Ti 3p
Ti 3d
V
V 3s
V 4s
V 3p
V 3d
(e)
(f)

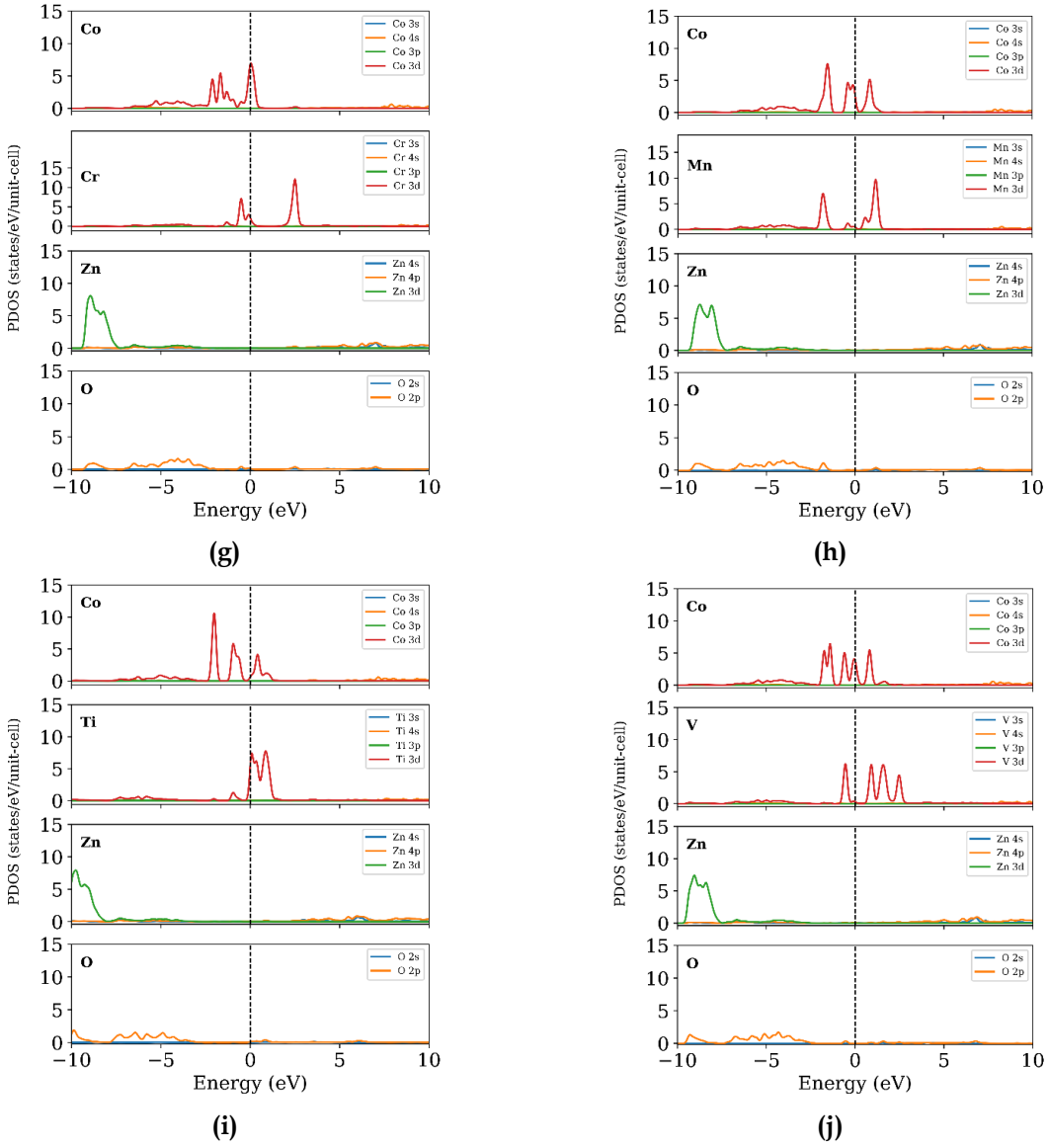

Figure 5. PDOS of Co-doped ZnO showing the orbital contributions of Co, O, and Zn atoms based on (a) DFT calculations, and (b) DFT+U calculations, with a U value of 4 eV applied to Zn and Co. PDOS of CoX-doped ZnO calculated using DFT, where X = (c) CoCr, (d) CoMn, (e) CoTi, and (f) CoV. PDOS of CoX-doped ZnO calculated using DFT+U, with a U value of 4 eV applied to Zn, Co, and the dopant atom X, where X = (g) CoCr, (h) CoMn, (i) CoTi, and (j) CoV. The correction introduces shifts in the localized *d*-orbitals

As shown in Figure 5(a–b), the PDOS of ZnO doped with Co, calculated using standard DFT and DFT+U (U = 4 eV for Zn and Co), reveals notable differences in the electronic structure. In standard DFT, the conduction band partially overlaps with the Fermi level, indicating a metallic-like behavior and the collapse of the semiconducting gap. Applying the DFT+U correction shifts the localized *d*-orbitals of Co and Zn, slightly restoring the gap; however, residual states persist near the Fermi level. These states are likely derived from Co *3d* orbitals interacting with O *2p* states, suggesting strong hybridization effects that hinder the formation of a full band gap.

Furthermore, Figures 5(c–f) and 5(g–j) present the PDOS of CoX-doped ZnO (X = Cr, Mn, Ti, V) under DFT and DFT+U, respectively. The introduction of X modifies the distribution of *d*-states near the Fermi level, enhancing absorption in the visible range. Notably, DFT+U calculations indicate that applying U to the dopant X localizes the *d*-states further, shifting some occupied levels deeper and unoccupied levels higher, which correlates with the observed optical transitions. This orbital-resolved analysis reveals that the visible-region absorption primarily originates from transitions between the Co 3d and X 3d orbitals, involving O 2p states, which provides a mechanistic explanation for the codoping effect on ZnO's electronic and optical properties.

These interactions between the dopant *d*-states and the conduction or valence bands result in the formation of localized electronic states near the Fermi energy. These energy levels increase the density of states (DOS) and effectively suppress the formation of a distinct band gap. For instance, in CoCr and CoMn doping, the dopant *d*-states introduce multiple energy levels within the Fermi region, significantly disrupting the band structure. Similarly, CoTi and CoV codoping exhibit strong *d*-orbital overlap near the Fermi level, maintaining the metallic character of the material. Overall, the electronic behavior of these Co- and CoX-doped ZnO systems is largely governed by the dopant *d*-orbitals.

As shown in Figure 5(g–j), DFT+U corrections were applied to better understand the electronic behavior of dopant atoms in CoX-codoped ZnO. PDOS analysis identifies the orbital contributions near the Fermi level and explores how these are influenced by the atomic properties of each dopant, particularly their *d*-electron occupancy and position in the periodic table. The results reveal a clear distinction between the behavior of Cr and Mn, with atomic numbers 24 and 25, respectively, and Ti and V, with atomic numbers 22 and 23, respectively. Cr and Mn show significant *d*-orbital contributions at both the valence band maximum and the conduction band minimum, indicating a broader energy distribution of *d*-states and stronger interaction with the ZnO host lattice. In contrast, Ti and V, which have fewer *d*-electrons, exhibit PDOS peaks below the Fermi level at lower energies, suggesting that the DFT+U correction induces a larger energetic shift in these less-occupied orbitals.

Band structure, DOS, and PDOS analyses based on DFT and DFT+U calculations confirm that transition metal codoping introduces mid-gap states and perturbs the electronic density around the Fermi level. The systematic underestimation of the band gap in both DFT and DFT+U, compared to experimental results, is primarily attributed to their inherent limitations in describing electron correlation effects within localized *d*-orbitals, particularly those associated with transition metal dopants.

In this study, such limitations are evident in ZnO doped with Co. Zn, with a [Ar] $3d^{10}4s^2$ electronic configuration, possesses a fully occupied *3d*-orbital lying deep in the valence band, which does not significantly contribute to states near the Fermi level. In contrast, Co, with a [Ar] $3d^7 4s^2$ configuration, has partially filled *3d*-orbitals, resulting in the emergence of Co-derived *3d*-states near the Fermi level. These states appear as nearly flat bands in the band structure, reflecting their localized character. A similar behavior is observed for other transition metals such as Cr, Mn, Ti, and V, which introduce localized *3d*-states whose positions relative to the Fermi level depend on their electron configuration and degree of *d*-orbital occupancy.

Such localized and partially filled *3d*-states are challenging for standard DFT to describe accurately due to self-interaction errors and the neglect of dynamic many-body correlations. The flatness of these bands, indicating the coexistence of occupied and unoccupied *3d*-states near the Fermi energy, is consistent with previous reports on transition metal doping in wide-bandgap semiconductors. While DFT+U introduces a static on-site Coulomb correction to partially mitigate these deficiencies, it still cannot fully capture electron-electron interactions in these systems, resulting in underestimated band gaps relative to experiments. These findings underscore the need for employing more advanced approaches, such as hybrid functionals or the GW approximation (G = Green's function, W = screened Coulomb interaction), to obtain quantitatively accurate electronic structures in transition metal-doped oxides [38].

Optical Properties

The optical properties of a material are fundamentally governed by its electronic structure, as they determine the material's ability to interact with electromagnetic radiation. In this work, although no direct simulation of device performance is conducted, the optical characteristics of the material suggest its potential applicability in optoelectronic devices. These properties were derived from the complex dielectric function $\varepsilon(\omega)$, which was calculated using both standard DFT and the DFT+U method. The inclusion of the Hubbard U correction provides a more accurate description of the interband transitions involved in optical processes.

The open paren omega close paren and the imaginary part script epsilon sub 2 dielectric function $\varepsilon(\omega)$ comprises the real part $\varepsilon_1(\omega)$ and the imaginary part $\varepsilon_2(\omega)$. $\varepsilon_1(\omega)$ describes the dispersive response of the material, reflecting its ability to be polarized by an external electric field and its contribution to the refractive index, while $\varepsilon_2(\omega)$ represents the absorptive response and indicates the probability of photon-induced electronic transitions between the valence and conduction bands. Together $\varepsilon_1(\omega)$ and $\varepsilon_2(\omega)$ determine key optical properties, including the refractive index, reflectivity, and absorption coefficient, highlighting the tunability of ZnO's optical behavior through CoX codoping. For semiconductors, $\varepsilon_1(\omega)$ typically exhibits a high value at low photon energies and gradually decreases with increasing energy, whereas $\varepsilon_2(\omega)$ presents characteristic peaks corresponding to specific interband transitions. In contrast, metallic systems show a steep increase in $\varepsilon_1(\omega)$ at very low photon energies due to free-carrier screening, and $\varepsilon_2(\omega)$ lacks a sharp onset, instead rising continuously across low-energy regions. This is indicative of intraband transitions. Such behavior is observed in the Co and CoX-doped ZnO systems, confirming the metallic-like optical response introduced by transition metal *d*-states.

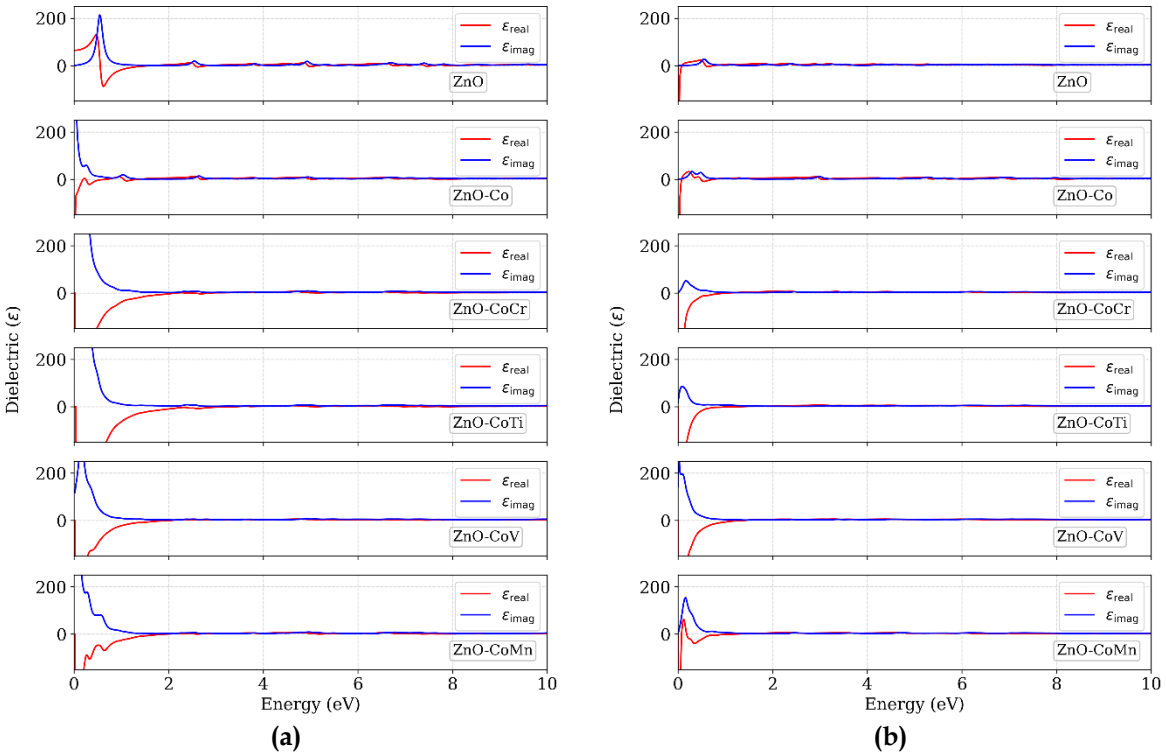

Figure 6. Dielectric constant of pure ZnO and CoX codoped ZnO calculated using (a) DFT and (b) DFT+U method

As shown in Figure 6, the dielectric response of pristine ZnO displays typical semiconductor behavior: $\varepsilon_1(\omega)$ starts from a high value at low energy and decreases smoothly, while $\varepsilon_2(\omega)$ shows sharp peaks that mark the onset of electronic transitions. However, when ZnO-Co and ZnO-CoX (X = Cr, Mn, Ti, V), the dielectric behavior changes significantly. These changes in the dielectric function originate from transitions involving the dopant *d*-states near the Fermi level, which introduce additional electronic states in the band gap. Such transitions enhance absorption at low photon energies, contributing to the observed metallic-like optical response. $\varepsilon_1(\omega)$ begins to increase from very low photon energies, and $\varepsilon_2(\omega)$ no longer shows a distinct onset but increases gradually, reflecting the presence of mid-gap states and a more metallic-like optical response. The absorption coefficient $\alpha(\omega)$, which quantifies how much light is absorbed per unit length of the material, was obtained from $\varepsilon_2(\omega)$ through the standard relation in linear response theory. The variations in $\varepsilon_1(\omega)$ and $\varepsilon_2(\omega)$ Due to doping, as shown in Figure 11, illustrates the tunability of ZnO's optical behavior, particularly in the low-energy region. This tunability is crucial for designing materials with tailored optical characteristics for potential applications in optoelectronic devices. The optical response, as revealed by the dielectric function, highlights the sensitivity of ZnO to electronic modifications introduced through the doping of transition metals.

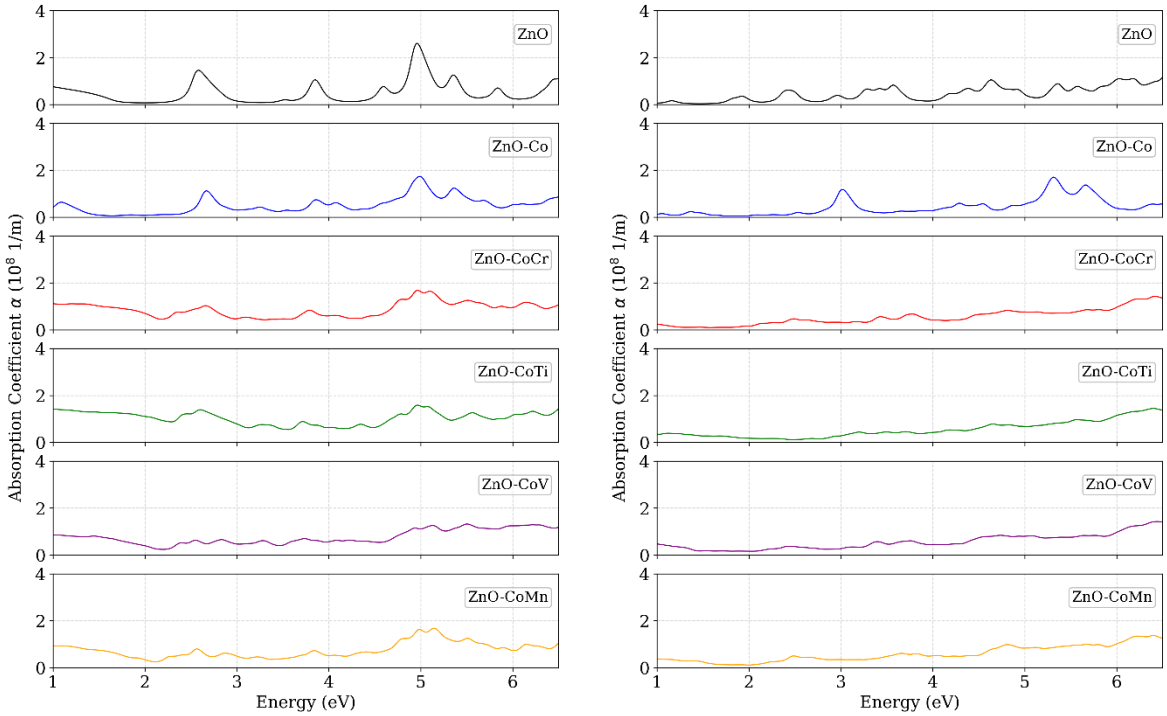

Figure 7. Absorption coefficient of ZnO and CoX codoped ZnO calculated using (a) DFT and (b) DFT+U correction.

The absorption for pristine and co-doped ZnO systems is presented in Figure 7. Incorporating the DFT+U correction adjusts the position of strong interactions and shifts the absorption onset toward higher energies, producing results that align more closely with experimental trends. Across all systems, the main interband transitions begin near 3 eV. These additional absorption peaks originate from electronic transitions involving dopant *d*-states and their hybridization with O 2*p* states, which introduce mid-gap states and extend light absorption into the visible region. For pure ZnO, the absorption occurs predominantly in the ultraviolet (UV) region, with peaks below 400 nm. In contrast, codoping with Co and other transition metals, such as Cr, Mn, Ti, and V, introduces additional absorption in the 400–500 nm range, thereby enhancing light capture in the visible region.

The optical absorption peak is a critical indicator of a material's ability to absorb light efficiently at specific photon energies. Semiconductors like ZnO inherently absorb strongly in the UV and near-visible regions. Table 2 presents a comparison of the absorption peak positions for pristine ZnO, ZnO doped with Co, and ZnO codoped with CoX. A consistent redshift is observed with increasing dopant complexity, indicating enhanced photon absorption capability in the visible range.

Based on Table 2, the comparison of optical absorption peaks for ZnO co-doped with CoX reveals two distinct regions. The primary absorption peak is clearly observed in the ultraviolet (UV) region, specifically below 380 nm. This result is consistent with both experimental findings and previous computational studies. Furthermore, the introduction of dopants in ZnO-Co or ZnO-CoX (X = Cr, Mn, Ti, V) leads to the emergence of secondary peaks in the higher wavelength range, particularly within the visible light spectrum. These additional peaks suggest enhanced absorption in the visible region, indicating that codoping

not only modifies the band structure but also enhances the material's potential for optoelectronic applications, particularly in devices such as solar cells.

The enhanced absorption in the visible region observed upon CoX codoping can be attributed to orbital-level interactions between the transition-metal dopants and the ZnO host lattice. As revealed by the PDOS analysis in Figure 5, the introduction of Co and X (Cr, Mn, Ti, and V) generates localized 3*d* states near the Fermi level, mainly originating from the partially filled d orbitals of the dopants. These states act as intermediate energy levels that facilitate optical transitions between the O 2*p*-derived valence band and the dopant 3*d* conduction sublevels. For instance, in Co–Cr and Co–Mn systems, the Cr^{3+} ($3d^5$) and Mn^{2+} ($3d^5$) ions contribute to visible-light absorption through d transitions between the spin-split e_g and t_{2g} states, whereas in Co–Ti and Co–V systems, hybridization between Co 3*d*, Ti 3*d*, and V 3*d* orbitals introduces shallower donor-like states near the conduction band. These orbital interactions effectively reduce the transition energy, shifting the absorption edge to lower photon energies, which is consistent with the observed redshift in the absorption spectra. Thus, the enhanced absorption in the visible region is a direct consequence of the dopant-induced intra-*d* and *p*–d transitions, which broaden the range of optically active states within the ZnO band gap. These mid-gap states arising from dopant *d*-orbitals are responsible for the redshift in absorption peaks, as summarized in Table 2.

Table 2. Comparison of optical absorption peak of ZnO, ZnO-Co, and ZnO-CoX.

Material	Method	Absorption Peak (eV)		Reference
		Ultraviolet (Primary)	Visible Light (Secondary)	
ZnO	DFT	310	563	[39]
ZnO	DFT	113	-	[34]
ZnO	DFT+U	82,67	-	[34]
ZnO	Experiment	390	-	[40]
ZnO	DFT	166	479	This Research
ZnO	DFT+U	161	511	This Research
ZnO-Co	Experiment	-	520	[40]
ZnO-Co	DFT	<200	-	[12]
ZnO-Co	DFT	182	465	This Research
ZnO-Co	DFT+U	154	409	This Research
ZnO-CoCr	DFT	169	465	This Research
ZnO-CoCr	DFT+U	155	498	This Research
ZnO-CoMn	DFT	169	483	This Research
ZnO-CoMn	DFT+U	124	498	This Research
ZnO-CoTi	DFT	123	475	This Research
ZnO-CoTi	DFT+U	123	401	This Research
ZnO-CoV	DFT	124	438	This Research
ZnO-CoV	DFT+U	161	511	This Research

The shaded regions in blue represent the UV range with wavelengths below ~380 nm, while the yellow regions indicate the visible light range 380–800 nm. In the DFT-based results, as shown in Figure 8(a), pristine ZnO exhibits two major absorption peaks at approximately 166 nm in the UV region and 479 nm in the visible region. ZnO-doped Co doping shifts the first peak slightly to 182 nm and the second to 465 nm in the visible region. The ZnO CoCr has a strong UV absorption at 169 nm and a visible peak at 465 nm. The ZnO CoMn system features

peaks at 169 nm and 483 nm. The ZnO CoTi yields a strong UV absorption at 123 nm and a visible peak at 475 nm. Meanwhile, ZnO CoV exhibits a sharp UV peak at 124 nm and a visible peak at 438 nm, with the latter being the highest redshift among all doped samples in the visible range.

In the DFT+U results, as shown by the peak positions of pristine ZnO, there are absorption peaks at wavelengths under 161 nm in the UV and 511 nm in the visible. For Figure 8(b), ZnO-doped Co doping shifts the first peak slightly to 154 nm and the second to 409 nm in the visible region. The ZnO CoCr has a strong UV absorption at 155 nm and a visible peak at 498 nm. The ZnO CoMn system exhibits peaks at wavelengths of under 124 nm and 498 nm. The ZnO CoTi yields a strong UV absorption at 123 nm and a visible peak at 401 nm. Meanwhile, ZnO CoV exhibits a sharp UV peak at a wavelength of under 161 nm and a visible peak at 511 nm, confirming an effective redshift in the visible absorption band. These results highlight the critical role of transition metal doping in tuning the optical response of ZnO. In particular, codoping combinations such as CoCr and CoMn extend the absorption into longer visible wavelengths, thereby enhancing solar light harvesting potential.

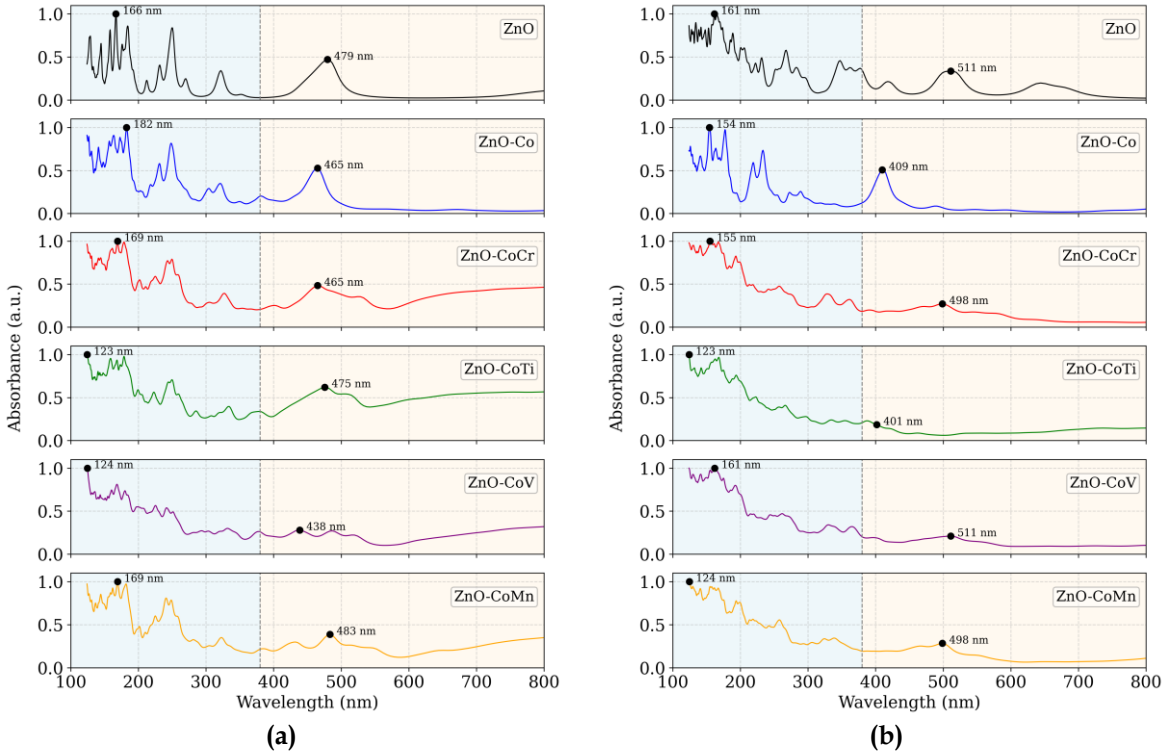

Figure 8. Absorbance spectra of ZnO and CoX codoped ZnO calculated using (a) DFT and (b) DFT+U correction.

Transition-metal codoping effectively modifies the optical characteristics of ZnO, improving its visible-light absorption. The DFT+U method significantly refines spectral predictions, particularly in terms of band gap positioning and transition accuracy. These findings support the strategic use of codoped ZnO for optoelectronic applications, particularly in solar energy harvesting and photocatalysis. The results confirm that transition metal *d*-orbitals play a decisive role in modulating interband optical transitions in ZnO. Moreover, beyond

absorption, CoX codoping can also modify other optical properties, including the refractive index and reflectivity, highlighting the broader tunability of ZnO's optical response for targeted optoelectronic applications.

Conclusion

The present study demonstrates that the codoping of ZnO with Co and transition metals significantly modifies its electronic and optical properties. The incorporation of 3*d* dopant states near the Fermi level introduces metallic-like behavior characterized by the appearance of flat bands and enhanced orbital hybridization, indicating partial bandgap closure compared to pristine ZnO. These electronic modifications lead to a visible-range shift in the absorption edge and an overall enhancement in optical absorption intensity, particularly for Co–Mn and Co–V codoped ZnO systems. This behavior underscores the crucial role of dopant chemistry in shaping the optoelectronic response of ZnO. Although the DFT+U scheme adequately captures relative codopant trends, its tendency to underestimate the absolute bandgap suggests that future investigations employing hybrid-functional or many-body perturbation methods (e.g., HSE06 or GW) would be beneficial for quantitative prediction. Overall, these findings offer valuable insights into the rational design of doped ZnO semiconductors and highlight their promising prospects in visible-light photocatalysis, solar energy conversion, and optoelectronic applications, where bandgap reduction and enhanced absorption directly translate to improved photon utilization efficiency.

Acknowledgment

This research was financially supported by the Ministry of Higher Education, Science, and Technology (KEMDIKTISAINTEK) under Grant No. 1483c/IT9.2.1/PT.01.03/2025 through the "Hibah BIMA Skema Penelitian Tesis Magister 2025" program. The authors thank Vast.ai for providing cloud computing resources utilized for the DFT calculations. We also acknowledge the use of OpenAI's ChatGPT for assistance in improving the clarity of the manuscript.

References

[1] Kementerian Energi dan Sumber Daya Mineral, "Peraturan Menteri ESDM No. 9 Tahun 2023". Jakarta, Indonesia: KESDM, 2024.

[2] H. B. Tambunan, "Sistem Pemangkit Listrik Tenaga Surya". Jakarta, Indonesia: Prenadamedia Group, ISBN 9786230221088, 2020, pp. 5–9.

[3] International Energy Agency, "World Energy Outlook 2010," *Energy Supply and Demand: Trends and Prospects*. Paris, France: IEA, 2010, pp. 5–20.

[4] D. Timmons, J. M. Harris, and B. Roach, "The Economics of Renewable Energy", *Renewable Energy Sources,* 2014, pp. 6–14.

[5] Kholiq, I. Editorial Board. *Current Opinion in Environmental Sustainability*, vol.4, no.1, 2012. ISSN 1877-3435.

[6] G. Widayana, "Pemanfaatan Energi Surya," *Jurnal Pendidikan Teknologi Dan Kejuruan*, vol. 9, no. 1, pp. 14–19, 2012.

[7] R. Fakharuddin, T. M. Jose, F. F. Brown, F. Santiago, and J. Bisquert, "A Perspective On the Production of Dye-Sensitized Solar Modules," *Energy & Environmental Science*, vol. 7, pp. 3952–3981, 2014.

[8] Q. Fu, X. Tang, B. Huang, T. Hu, L. Tan, L. Chen, and Y. Chen, "Recent Progress on the Long-Term Stability of Perovskite Solar Cells," *Advanced Science*, vol. 5, no. 5, 2018. Art. no. e1700387.
[9] Hardani, "Dye-Sensitized Solar Cell: Teori and Aplikasi", *Pustaka Ilmu*, 2019, ISBN 978-623-7066-12-5.
[10] A. M. Ali, A. A. Ismail, R. Najmy, and A. Al-Hajry, "Preparation and characterization of ZnO–SiO2 thin films as highly efficient photocatalysts," *Journal of Photochemistry and Photobiology A: Chemistry*, vol. 275, pp. 37–46.
[11] S. M. Lam, J. C. Sin, A. Z. Abdullah, and A. R. Mohamed, "Degradation of wastewaters containing organic dyes photocatalysed by zinc oxide: a review," *Desalination and Water Treatment*, vol. 41, no. 1–3, pp. 131–169, 2012.
[12] R. A. Soussi et al., "First Principal Study of Structural, Electronic, Optical Properties of co-doped ZnO," *Journal of Composites Science*, vol. 7, p. 511, 2023.
[13] Y. Liu, Q. Hou, S. Sha, and Z. Xu, "Electronic structure, optical and ferromagnetic properties of ZnO co-doped with Ag and Co according to first-principles calculations," *Vacuum*, vol. 173, pp. 145–157, 2020.
[14] Y. Sharma, V. Anand, and P. Heera, "Ab Initio Study of Structural and Magnetic Properties of Cobalt Doped Zinc Oxide," *J. Cond. Matt*., vol. 1, no. 2, pp. 48–51, 2023.
[15] J. Ma, W. Zhang, J. Lin, et al., "Theoretical study on group III elements and F co-doped ZnO," *Journal of Alloys and Compounds*, vol. 819, pp. 49–61, 2020.
[16] S. Xue, L. Zhang, G. Liu, Q. Wu, J. Ning, B. Zhang, et al., "Electronic Structures and Magnetic Properties of Co/Mn Co-Doped ZnO Nanowire: First-Principles LDA+U Studies," *Coatings,* vol. 13, no. 567, pp. 67–74, 2023.
[17] U. Haq, R. Ahmed, S. Goumri-Said, A. Shaari, and A. Afaq, "Electronic structure engineering of ZnO with the modified Becke-Johnson exchange versus the classical correlation potential approaches," *Phase Transitions*, vol. 86, pp. 1167–1177, 2013.
[18] M. V. Gallegos, C. R. Luna, M. A. Peluso, L. C. Damonte, J. E. Sambeth, and P. V. Jasen, "Effect of Mn in ZnO using DFT calculations: Magnetic and electronic changes," *Journal of Alloys and Compounds*, vol. 795, pp. 89–101, 2019.
[19] Y. Zhang, Y. Wang, and H. Zhang, "Magnetic properties of two-dimensional materials: A first-principles study," *Nature Communications*, vol. 6, no. 1, pp. 10012, 2015.
[20] M. Khuili, N. Fazouan, H. A. El Makarim, E. H. Atmani, A. Abbassi, and D. P. Rai, "(Li,F) co-doped ZnO: Optoelectronic devices applications," *Superlattices and Microstructures*, vol. 145, 2020.
[21] V. Christhunathan, P. Farràs, and M. Tong, "First-principles study of electronic properties of Zn and La doped and co-doped anatase TiO2," *AIP Advances*, vol. 13, no. 125013, 2023.
[22] A. Latif, M. Mohsin, I. A. Bhatti, A. A. Tahir, M. T. Hussain, and J. Iqbal, "Experimental and ab initio studies of Co-doped ZnO nanophotocatalyst thin films for dye mineralization," *RSC Advances*, vol. 13, 2023.
[23] H. Takayama, K.-P. Bohnen, and F. Fulde, "Magnetic surface anisotropy of transition metals," *Physical Review B,* vol. 14, no. 4, pp. 1446–1449, 1976.
[24] M. Yaakob, N. H. Hussin, T. I. T. Kudin, O. Hassan, A. M. M. Ali, and M. Z. A. Yahya, "First Principles LDA plus U Calculations for ZnO Materials," *Integrated Ferroelectrics*, vol. 155, 2014.
[25] M. Fox, *Optical Properties of Solids*, 2nd ed., Oxford University Press, 2001, ch. 1

[26] M. O. Steinhauser and S. Hiermaier, "A review of computational methods in materials science: examples from shock-wave and polymer physics," *International Journal of Molecular Sciences*, vol. 10, no. 12, pp. 5135–5216, 2009.
[27] P. L. Mecci, A. Monica, I. R. Sinurat, A. Widiyani, A. Rajak, and I. Pardede, "First-Principles Study of Magnetic Anisotropy Energy In Two-Dimensional Ferromagnetic CrI3," *Indonesian Physical Review*, vol. 6, no. 1, pp. 60–84, 2023.
[28] I. Pardede, D. Yoshikawa, T. Kanagawa, N. Ikhsan, I. Murata, M. Obata, and T. Oda, "Anatomy of large perpendicular magnetic anisotropy in free-standing Co/Ni (111) multilayer," *Journal of Magnetism and Magnetic Materials*, vol. 500, p. 166357, 2020.
[29] H. Prayoga, Y. Yulianti, and A. Riyanto, "Analisis Dinamika Molekul Protein Lysozyme Putih Telur Dengan Model Potensial Lennard-Jones Menggunakan Aplikasi Gromacs," *Jurnal Teori dan Aplikasi Fisika*, vol. 6, no. 2, pp. 239–247, 2019.
[30] Ü. Özgür et al., "A comprehensive review of ZnO materials and devices," *Journal of Applied Physics*, vol. 98, no. 4, Art. no. 041301, 2005.
[31] N. T. Hung, A. R. T. Nugraha, and R. Saito, Quantum ESPRESSO Course for Solid-State Physics. Singapore: Jenny Stanford Publishing, 2023.
[32] Kubler, J. *International Series of Monographs on Physics*. New York: Oxford University Press; 2000
[33] Materials Project. *Material ZnO*. https://next-gen.materialsproject.org/materials/mp-2133
[34] K. Harun, N. A. Salleh, B. Deghfel, M. K. Yaakob, and A. A. Mohamad, "DFT + U calculations for electronic, structural, and optical properties of ZnO wurtzite structure: A review," *Results in Physics*, vol. 16, p. 102829, Mar. 2020
[35] M. Julita, M. Shiddiq, and M. Khair, "Determination of Band Gap Energy of ZnO/Au Nanoparticles Resulting in Laser Ablation in Liquid," *Indo. J. Chem. Res.*, vol. 10, no. 2, pp. 83–87, 2022.
[36] A. Rathor, V. Sharma, E. Chaturvedi, G. Sharma, and O. U. Okeke, "Electronic structure and magnetic properties of cobalt-doped zinc oxide," *J. Nano-Electron. Phys.*, vol. 3, no. 1, pp. 268–273, 2011, [Online]. Available: https://jnep.sumdu.edu.ua/en/full_article/170 (DOI not available).
[37] T. Thangeeswari, A. T. George, and A. A. Kumar, "Optical Properties and FTIR Studies of Cobalt Doped ZnO Nanoparticles by Simple Solution Method," *Indian J. Sci. Technol.*, vol. 9, no. 1, Jan. 2016.
[38] J. Doumont, F. Tran, and P. Blaha, "Limitations of the DFT-1/2 method for covalent semiconductors and transition-metal oxides," *Phys. Rev*. B, vol. 99, no. 11, pp. 115101, 2019.
[39] L. Chen, H. Hu, A. Wang, Z. Xiong, and Y. Cui, "Density functional theory study of adsorption of organic molecules on ZnO monolayers: Implications for conduction type and electrical characteristics," *Results Phys.*, vol. 56, Art. no. 107225, 2024.
[40] Y. Lu, Y. Lin, D. Wang, L. Wang, T. Xie, and T. Jiang, "A high-performance cobalt-doped ZnO visible light photocatalyst and its photogenerated charge transfer properties," *Nano Res.*, vol. 4, no. 11, pp. 1144–1152, 2011.